Fructose-2,6-bisphosphate restores TDP-43 pathology-driven genome repair deficiency in motor neuron diseases

Joy Mitra[a,†], Anirban Chakraborty[c,†], Vikas H. Malojirao[a], Manohar Kodavati[a], Santi M. Mandal[d], Velmarini Vasquez[a], Mikita Mankevich[d], Gourisankar Ghosh[d], Muralidhar L. Hegde[a,b,*], Tapas Hazra[c,*].

[a]Division of DNA Repair Research, Center for Neuroregeneration, Department of Neurosurgery, Houston Methodist Research Institute, Houston, TX 77030, USA
[b]Department of Neuroscience, Weill Cornell Medical College, New York, NY 10065, USA
[c]Department of Internal Medicine, University of Texas Medical Branch, Galveston, TX, 77555, USA
[d]Department of Chemistry and Biochemistry, University of California San Diego, LA Jolla, California 92093, USA

† These authors contributed equally.

*Address of corresponding authors:

Muralidhar L Hegde, PhD
Professor, Center for Neuroregeneration
Department of Neurosurgery
Houston Methodist Research Institute, Houston, Texas 77030, USA
Tel: (713) 441-7456
E-mail: mlhegde@houstonmethodist.org

Tapas Hazra, PhD
Professor, Department of Internal Medicine-Pulmonary, Critical Care & Sleep Medicine
University of Texas Medical Branch, Galveston, TX 77555, USA
Tel: (409) 772-6308
Fax: (409) 747-8608
E-mail: tkhazra@utmb.edu

Abstract
TAR DNA-binding protein 43 (TDP-43) proteinopathy plays a critical role in neurodegenerative diseases, including amyotrophic lateral sclerosis and frontotemporal dementia (FTD). In our recent discovery, we identified that TDP-43 plays a critical role in DNA double-strand break (DSB) repair via the non-homologous end joining (NHEJ) pathway. Here, we found persistent DNA damage in brains of ALS/FTD patients, primarily in the transcribed regions of the genome. We further investigated the underlying mechanism and found that the activity of polynucleotide kinase 3'-phosphatase (PNKP) was severely impaired in the nuclear extracts of both the patient brains and TDP-43-depleted cells. PNKP is a key player in DSB repair within the transcribed genome, where its 3'-P termini processing activity is crucial for preventing persistent DNA damage and neuronal death. The inactivation of PNKP in ALS/FTD was due to reduced levels of its interacting partner, phosphofructo-2-kinase fructose 2,6 bisphosphatase (PFKFB3), and its biosynthetic product, fructose-2,6-bisphosphate (F2,6BP), an allosteric modulator of glycolysis. Recent work from our group has shown that F2,6BP acts as a positive modulator of PNKP activity *in vivo*. Notably, exogenous supplementation with F2,6BP restored PNKP activity in both nuclear extracts from ALS/FTD brain samples and in patient-derived induced pluripotent stem (iPS) cells harboring pathological mutations. Our findings underscore the possibility of exploring the therapeutic potential of F2,6BP or its analogs in TDP-43 pathology-associated motor neuron diseases.

Keywords: TDP-43, PNKP, DNA damage, amyotrophic lateral sclerosis, PFKFB3.

Introduction

Amyotrophic lateral sclerosis and frontotemporal dementia (FTD) are neurodegenerative diseases marked by dysfunction and toxicity of TAR DNA-binding protein 43 (TDP-43), which drives progressive neuronal degeneration (1-5). TDP-43 pathology in these diseases is characterized by the loss of nuclear TDP-43 and its accumulation in the cytoplasm, disrupting cellular pathways in motor neurons (6, 7). Our recent studies demonstrated that TDP-43 plays a key role in the classical non-homologous end joining (C-NHEJ) pathway, which is primarily responsible for repairing DNA double-strand breaks (DSBs) in neurons. Upon DNA damage, TDP-43 is rapidly recruited at DSB sites, where it stably interacts with DNA damage response (DDR) and NHEJ factors, facilitating the recruitment of break-sealing XRCC4-Lig4 complex in induced pluripotent stem cell (iPSC)-derived motor neurons (5, 8-12). We found that mislocalization of ALS-associated mutant TDP-43 significantly impairs NHEJ-mediated DNA repair, leading to accumulation of DNA damage, cellular senescence, and increased neuroinflammation (13). Notably, the compromised NHEJ repair in TDP-43 proteinopathy is associated with reduced recruitment of XRCC4/Lig4 at DSB sites (5, 10), though the precise mechanism by which TDP-43 regulates C-NHEJ remains unclear.

In ALS and FTD cases, enhanced production of reactive oxygen species (ROS) and persistent inflammation can lead to oxidative genome damage and DNA single-strand (SSB) and double-strand breaks (DSBs) (14-18). Polynucleotide kinase 3'-phosphatase (PNKP) is a bifunctional DNA end-processing enzyme with 3'-phosphatase and 5'-kinase activities (19, 20), and is a major 3'-phosphatase that is involved in both DNA BER/SSB and C-NHEJ-mediated DSB repair pathways in mammalian cells (21-24). Importantly, functional loss of PNKP in neuronal cells has been linked to several neuropathological conditions (25-30). Additionally, we have shown that PNKP plays a critical role in preferential repair of actively transcribed genomes via TC-SSBR and TC-NHEJ pathways, respectively (11, 12, 31-33). 3´-phosphatase activity of PNKP

is severely compromised in two most prevalent polyQ neurodegenerative diseases, Huntington's disease (HD) (34) and spinocerebellar ataxia type 3 (SCA3) (32, 35).

Several studies provide strong mechanistic evidence linking metabolic reprogramming and DNA repair activity through the direct involvement of metabolic enzymes and metabolites, regulation of dNTP pool, and metabolic regulation of epigenetic remodeling (36). The homodimeric 6-phosphofructo-2-kinase/fructose-2,6-bisphosphatases (PFKFBs) are the key glycolytic enzymes, which mediate the rate-limiting step in the process (37). Recently, PFKFB3 is found to be translocated to the nucleus (38). Role of PFKFB3 in DSB repair via HR pathway also has been demonstrated (39). To further investigate the molecular basis of PNKP inactivation in HD and SCA3, we observed that PNKP interacts with PFKFB3 and elucidated PFKFB3's role in TC-NHEJ. Notably, the levels of both PFKFB3 and its product, fructose-2,6 bisphosphate (F2,6BP), an allosteric modulator of glycolysis, are significantly lower in the nuclear extracts of post-mortem HD and SCA3 patient brains. Supplementation of F2,6BP in HD mouse striatal neuronal cells and in HD flies fully restored nuclear and mitochondrial genome integrity and functionality (35, 40), suggesting F2,6BP to be a positive regulator of PNKP activity in vivo. Reduced level of PFKFB3 is therefore linked to decreased PNKP activity in HD and SCA3, connecting metabolic processes to DNA repair (32, 35).

Since TDP-43, PNKP and PFKFB3 are involved in NHEJ-mediated DSB repair, we investigated the role of PNKP and PFKFB3 in ALS and FTD models of TDP-43 pathology. We indeed observed a near-complete loss of 3'-phosphatase activity of PNKP, but not the protein level, in TDP-43-associated neurodegenerative conditions, correlating with TDP-43 mislocalization and persistent DNA damage. Notably, reduced PFKFB3 and F2,6BP levels have been observed in ALS/FTD patient tissues, indicating potential disruptions in glycolytic pathways that may exacerbate genomic instability associated with TDP-43 pathology. Importantly, such PNKP-mediated repair deficiency could be restored by exogenous supplementation of F2,6BP in extracts from ALS/FTD patient brains and patient-derived iPSCs. Overall, our findings highlight the therapeutic potential of F2,6BP or its analogs in ALS/FTD and other neurodegenerative diseases associated with TDP-43 pathology.

Methods

Cell culture and Stable Line Generation

Human embryonic kidney HEK293 (ATCC) cells were cultured in Dulbecco's modified Eagle's medium (DMEM) with high glucose, supplemented with 10% fetal bovine serum (FBS) and 100 U/ml penicillin-streptomycin in a humidified chamber at 37°C and 5% CO_2.

To generate the PNKP-FLAG-expressing stable HEK293 cell line, coding DNA sequence of human PNKP (GenBank BC033822.1) was re-cloned to pFLAG-cDNA (Invitrogen/Life Technologies) between Pcmv and FLAG-tag encoding sequences within HindIII and BamHI sites. The gene in the newly constructed plasmid carried the natural Kozak sequence and nucleotides 97–1,669 of PNKP cDNA. The region containing Kozak-PNKP-FLAG was then transferred to pcDNA3.1-Hygro (Invitrogen/Life Technologies) within the HindIII-XbaI unique vector sites to generate the final plasmid, which was then used for creating a stable cell line resistant to hygromycin (Hygro), following standard procedures (21). Ectopic expression of PNKP was confirmed by western blotting of whole-cell extract using anti-FLAG Ab (Sigma, F1804).

siRNA transfection

TDP-43 depletion was carried out in HEK293 cells using siRNAs (80 nM; transfected twice on consecutive days) against *TARDBP* gene. The cells were transfected with control siRNA (siControl) or TDP-43-specific siRNA (siTDP-43; Thermo Fisher; Silencer Select; 4392420) using lipofectamine 3000 (Invitrogen) for 6 h in optiMEM (Gibco; reduced serum media, 11058021), followed by replacing the medium with DMEM-High Glucose complete medium. Nuclear extracts were prepared from the harvested cells (72-96 h post-transfection) to examine the depletion of individual proteins by immunoblot (IB) analysis using specific antibodies. Lamin-B was used as the nuclear loading control.

Neural Progenitor Stem Cell (NPSC) Induction

Control and TDP-43 mutant induced pluripotent stem cells (iPSCs) were cultured on basement membrane matrix Geltrex LDEV-Free-coated Petri dishes using 1X Essential 8 media (Gibco, A1517001) and maintained in a humidified incubator at 37°C in 5% CO_2. To derive NPSCs, PSC neural induction media (Gibco A1647801) was used as per the manufacturer's protocol. The process involved replacing the Essential 8 media with PSC neural induction media approximately 24 h after sub-platting those iPSCs. This media was maintained for 7 days. The first passage (P0) NPSCs were then transferred onto Geltrex (Gibco, A1413201) coated 6-well plates and cultured in StemPRO neural stem cell SFM media (Gibco, A1050901). Neural induction efficiency was assessed at third passage by immunofluorescence (IF) staining.
ALS-related TDP-43 G287S mutant and its CRISPR/Cas9-corrected isogenic TDP-43 S287G as well as FTD-related TDP-43 A382T along with C9ORF72 repeat mutation carrying iPSCs were kindly gifted by our collaborators Drs. Van Damme and Van Den Bosch (University of Leuven, Belgium). These lines were cultured according to their published protocol (41). Control and ALS patient-derived TDP-43 G298S mutant iPSC (NINDS, NH50216) lines were purchased from NIH-NINDS (42). Engineered homozygous TDP-43 Q331K mutant (Jax, JIPSC1064) and its isogenic control (Jax, JIPSC1104) lines were purchased from Jax iPSC.

Motor Neuron Differentiation

Motor neurons were generated from patient and control subject-derived iPSCs (NIH-NINDS & VIB-KU Leuven). The differentiation process followed established protocols with some modifications (43, 44). In brief, iPSC clones were transferred from a 60-cm dish to a T-25 flask filled with neuronal basic medium. The medium consisted of a mixture of 50% Neurobasal medium (Gibco, 21103049) and 50% DMEM/F12 medium (Gibco, 21331020), supplemented with N2 and B27 supplements without vitamin A. Collagenase type IV digestion was performed to facilitate suspension of the iPSC clones. Afterward, the suspended cell spheres were subjected to a series of incubations. Initially, they were treated with various inhibitors including 5 μM ROCK Inhibitor (Y-27632), 40 μM TGF-β inhibitor (SB 431524), 0.2 μM bone morphogenetic protein inhibitor (LDN-193189), and 3 μM GSK-3 inhibitor (CHIR99021). This was followed by incubation in a neuronal basic medium containing 0.1 μM retinoic acid (RA) and 500 nM Smoothened Agonist (SAG) for 4 days. Subsequently, the cell spheres were incubated for 2 days in a neuronal basic medium containing RA, SAG, 10 ng/ml Brain-derived neurotrophic factor (BDNF), and 10 ng/ml Glial cell-derived neurotrophic factor (GDNF). To dissociate the cell spheres into single cells, they were exposed to a neuronal basic medium containing trypsin (0.025%)/DNase in a water bath at 37°C for 20 min. Afterward, the cells were pipetted into a medium containing trypsin inhibitor (1.2 mg/ml) to maintain their viability. Following cell counting, a specific number of cells were seeded onto dishes or chamber slides coated with 20

μg/ml Laminin. These cells were incubated for 5 days in a neuronal basic medium containing RA, SAG, BDNF, GDNF, and 10 μM DAPT. Subsequently, the medium was switched to one containing BDNF, GDNF, and 20 μM Inhibitor of γ-secretase (DAPT) for an additional 2 days. For motor neuron maturation, the cells were cultured in a medium containing BDNF, GDNF, and 10ng/ml ciliary neurotrophic factor (CNTF) for a period exceeding 7 days.

Immunoblotting (IB)

For IB analysis, cell lysates extracted with 1x RIPA buffer (Millipore, 20-188) containing the protease inhibitor cocktail (Roche, 11836170001). Protein concentration was measured using 1x Bradford reagent (Biorad) in NanoDrop instrument. Then 20 μg protein per sample was loaded into NuPAGE 4–12% Bis-Tris precast (Invitrogen) gels for electrophoresis. After transfer to nitrocellulose membranes, the separated proteins were incubated with target primary and respective secondary antibodies, and the protein signals were detected by adding chemiluminescence reagents (LI-COR) and visualized by LI-COR Odyssey imaging system. HDAC2 and Lamin-B were used as loading controls as appropriate.

Co-immunoprecipitation (Co-IP)

Approximately 30 mg of brain tissues from ALS/FTD post-mortem patients or healthy controls (or ALS vs Sham mice brain cortices) were homogenized with 4 volumes of ice-cold homogenization buffer [0.25 M sucrose, 15 mM Tris-HCl, pH 7.9, 60 mM KCl, 15 mM NaCl, 5 mM EDTA, 1 mM EGTA, 0.15 mM spermine, 0.5 mM spermidine, 1 mM dithiothreitol (DTT), 0.1 mM phenylmethylsulfonyl fluoride (PMSF), and protease inhibitors (EDTA-free; Roche)]. Following homogenization, homogenate was incubated on ice for 15 min and centrifuged at 1,000×g to obtain the cell pellet. Cells were lysed in Buffer A [10 mM Tris-HCl (pH 7.9), 0.34 M sucrose, 3 mM $CaCl_2$, 2 mM magnesium acetate, 0.1 mM EDTA, 1 mM DTT, 0.5% Nonidet P-40 (NP-40) and 1X protease inhibitor cocktail (Roche)] and centrifuged at 3,500×g for 15 min. Nuclear pellets were washed with Buffer A without NP-40 and then lysed in Buffer B [20 mM HEPES (pH 7.9), 3 mM EDTA, 10% glycerol, 150 mM potassium acetate, 1.5 mM $MgCl_2$, 1 mM DTT, 0.1% NP-40, 1 mM sodium orthovanadate (vanadate) and 1X protease inhibitors] by homogenization. Supernatants were collected after centrifugation at 15,000×g for 30 min and DNA/RNA in the suspension was digested with 0.15 U/μl benzonase (Novagen, 70-746-3) at 37°C for 1 h. The samples were centrifuged at 20,000×g for 30 min, and the supernatants collected as NEs. Co-IP was performed using anti-PNKP (BioBharati Life Science, BB-AB0105) antibody with Protein A/G PLUS agarose beads (Santa Cruz Biotechnology, sc2003,) overnight, followed by four washes with Wash buffer [20 mM HEPES (pH 7.9), 150 mM KCl, 0.5 mM EDTA, 10% glycerol, 0.25% Triton-X-100 and 1X protease inhibitors] and eluted with Laemmli Sample Buffer (Bio Rad; final concentration 1X). The immunoprecipitates were tested for the interacting proteins using appropriate Abs [PFKFB3 (GeneTexGTX108335), Lig 4 (GeneTex, GTX108820), RNAP II (Biolegend, 920202, pSer2, H5 Ab), and TDP-43 (Protein tech, 10782-2-AP).

3´-phosphatase activity assay of PNKP

The PNKP 3´-phosphatase activity in 1 μg of nuclear extracts (NE) of post-mortem ALS/FTD and age-matched patients' cortical tissues or with purified recombinant PNKP (2 ng) was conducted, as described previously (35). Five pmol of the radiolabeled substrate was incubated at 37°C for 15 min in buffer A (25 mM Tris-HCl, pH 8.0, 100 mM NaCl, 5 mM $MgCl_2$, 1 mM DTT, 10% glycerol

and 0.1 μg/μl acetylated BSA). Five pmol of non-radiolabeled substrate was used as cold substrate. For in vitro PNKP restoration/abrogation, similar assays were done after incubation of F2,6BP/F6P/F1,6BP with the nuclear extracts for 15 min. The radioactive bands were visualized in PhosphorImager (GE Healthcare) and quantitated using ImageQuant software.

Enzymatic preparation of F2,6BP

Enzymatic preparations of F2,6BP were conducted, as we described earlier (35).

Estimation of F2,6BP in patient brain nuclear extracts

To quantify F2,6BP, the F6P assay kit (Sigma-Aldrich) was used to measure the amount of F6P before and after treating the crude nuclear extracts with 0.1M HCl and incubated at 37°C for 30 mins. Acid treatment converts F2,6BP into F6P. The assay was performed using manufacturer's protocol which uses NADH-linked luciferase bioluminescence (35).

Long amplicon quantitative PCR (LA-qPCR)

Genomic DNA was extracted from cultured cells or autopsied brain tissues using the Genomic tip 20/G kit (Qiagen) per the manufacturer's protocol, to ensure minimal DNA oxidation during the isolation steps. The DNA was quantitated by Pico Green (Molecular Probes) in a black-bottomed 96-well plate and gene-specific LA qPCR assays were performed as described earlier (35) using Long Amp Taq DNA Polymerase (New England Biolabs). POLB and RNAPII (12.1 and 11.3 kb) were amplified from the experimental and control samples using appropriate oligos. Enolase/NeuroD (transcribed genes) and MyH2/MyH4 (non-transcribed genes) were amplified from human post-mortem samples. The list primers used in this study is detailed in *Supplementary* **Table S2**.

The LA-qPCR reaction was set for all genes from the same stock of diluted genomic DNA (10-15 ng) sample, to avoid variations in PCR amplification during sample preparation. The final PCR reaction conditions were optimized at 94°C for 30 s; (94°C for 30 s, 55-60°C for 30 s depending on the oligo annealing temperature, 65°C for 10 min) for 25 cycles; 65°C for 10 min. Since amplification of a small region is independent of DNA damage, a small DNA fragment (~200-400 bp) from the corresponding gene(s) was also amplified for normalization of amplification of the large fragment. The amplified products were then visualized on gels and quantitated with ImageJ software (NIH).

Immunofluorescence (IF)

For NPSCs and motor neurons, the chamber slides were pre-coated with Geltrex and Matrigel, respectively, to facilitate cell adherence. Fixation of the cells for IF analysis was performed by replacing the media with a 1:1 ratio mixture of fresh media and 8% paraformaldehyde (PFA) in PBS, resulting in a final concentration of 4% PFA. Post-fixation, the slides were permeabilized using 0.2% Triton X-100 in 1X PBS, followed by blocking with 5% Goat Serum-TBS-T (1x TBS with 0.1% Tween-20) to prevent non-specific antibody binding. The cells were then incubated overnight at 4°C with target primary antibodies. Following this step, Alexa Fluor-488 (green) and 647 -conjugated secondary antibodies (Thermo Fisher) were incubated for 1 h, and slides were then mounted with coverslips after applying DAPI-containing mounting media (Sigma-Aldrich, USA) to visualize the nuclei. Imaging was performed using a Zeiss Axio Observer 7 microscope or an Olympus Flouview3000 confocal microscope.

Proximity ligation assay (PLA)
PLA was conducted to investigate direct protein-protein interactions within cells. Approximately 20,000 cells were seeded per well in 8-well chamber slides for this experiment. After staining, cells underwent a washing step and were then fixed with 4% PFA for 15 min at room temperature. Subsequent steps included permeabilization in 0.2% Triton X-100 in 1x PBS for 10 min at RT, followed by PBS washing to remove any residual permeabilization agent. The in-situ PLA experiment was performed per the manufacturer's guidelines, using the DuoLink kit (Sigma-Aldrich, USA). After the PLA procedure, coverslips were mounted using DAPI mounting media (Sigma-Aldrich, USA), and imaging was performed using either a Zeiss Axio Observer 7 microscope or an Olympus Flouview3000 confocal microscope.

Immunohistochemistry (IHC)
Tissue samples were paraffin embedded and sliced into 5 µm horizontal sections and mounted on glass slides. Slides were dewaxed and autoclaved for 10 min at 121°C in 0.01 M citrate buffer pH 6.0 for antigen retrieval. Immunostaining was performed using overnight incubation at 4°C with mouse anti-TDP-43 (R&D Systems, MAB77781, 1:200), and rabbit anti-phospho-TDP-43 (S409/410) (Proteintech, 80007-1-RR, 1:300). Nuclei were counter stained with DAPI. Slides were imaged on the next day in a confocal microscope.

Comet assay
The neutral comet assay was performed using the Comet Assay Kit (Trevigen, #4250-50-K), according to the manufacturer's protocol to assess the extent of DNA DSBs in each sample. Briefly, singlet cell suspension was prepared by trypsinization of respective cell types in DPBS buffer and about 200 cells were smeared in LMAgarose at 37°C in duplicate in each slide. The comet tails were visualized by staining the DNA with SYBR Green gold stain under a fluorescence microscope.

Statistical analysis
All data are expressed as mean ± standard deviation (SD). Comparisons among experimental groups were carried out using Student's t-test, one-way or two-way ANOVA, as appropriate, for significance. Statistical analyses were performed using GraphPad Prism version 10 software. A p-value of less than 0.05 was considered statistically significant.

Results and Discussion

PNKP Activity is Significantly Reduced in ALS and FTD Patient Tissues
While our recent studies demonstrate the accumulation of DNA DSBs and a deficiency in NHEJ-mediated DSB repair in ALS patient brains with TDP-43 pathology (5), the potential link between PNKP and TDP-43 has not been investigated in the context of DNA DSB repair. Therefore, we assessed the impact of TDP-43 pathology on PNKP's 3'-phosphatase activity under ALS and FTD conditions (*Supplementary* **Figure S1A**) using a duplex oligo-based *in vitro* assay as schematically shown in **Figure 1A**. We observed a significant inhibition of PNKP activity in nuclear extracts (NE) from ALS-TDP-43 (Lns 5-7) and FTD-TDP-43 (Lns 8-9) cortical tissues, compared to age-matched non-neurological controls (Lns 2-4) (**Figure 1B**). We further validated this observation exploiting a second cohort of Guamanian-ALS patients (Lns 6-9) and age-matched non-

neurological control (Lns 2-5) brain cortical tissues and found a significant and comparable reduction in fold change of PNKP activity between the Guamanian-ALS and sporadic ALS cohorts, reinforcing the association between TDP-43 pathology and impaired PNKP function (**Figure 1C**). Demographic descriptions of ALS, FTD patients and age-matched non neurological controls are detailed in *Supplementary* **Table S1**. Furthermore, we quantified relative PNKP levels in the analyzed patient specimens by immunoblotting (IB), which was largely unaffected compared to non-neurological controls (**Figure 1D**; *Supplementary* **Figure S1B**), indicating the loss of PNKP activity independent of its protein levels in ALS and FTD brains. These results collectively support the notion that PNKP dysfunction is prevalent in ALS and FTD with TDP-43 pathology.

Downregulation of TDP-43 Abolishes PNKP Activity in Cultured Neuronal Cells

To further elucidate the mechanism how PNKP activity might be regulated by functional loss of TDP-43, we performed TDP-43 siRNA (siTDP-43)-mediated knockdown (KD) of TDP-43 in HEK293 cells, which showed a significant KD of TDP-43 without affecting the PNKP protein level, compared to control siRNA (siControl)-treated cells (**Figure 2A**). Consistently, TDP-43 KD revealed a marked decrease in PNKP's 3'-phosphatase activity in siTDP-43 (Ln 4) compared to siControl (Ln 3) cells (**Figure 2B**). These findings indicate that the loss of TDP-43 directly affects PNKP's DNA end-processing functionality, independent of its expression levels, contributing to the observed accumulation of unrepaired DNA breaks in ALS and FTD.

PNKP Overexpression Rescues TDP-43 KD-Associated DNA Damage in Cells

To determine whether PNKP complementation can mitigate TDP-43 depletion-induced DNA damage, we transfected HEK293 cells ectopically expressing FLAG tagged-PNKP with siControl or siTDP-43 and compared the levels of DNA DSB marker γH2AX across the groups, revealing that PNKP overexpression (OE) significantly reduced γH2AX levels in siTDP-43 cells compared to respective control cells (**Figure 3A**). In addition, neutral comet assay under the same conditions as shown in **Figure 3A** demonstrated marked reduction in DNA DSB in terms of decreased comet tail moment in PNKP-OE + siTDP-43-treated cells compared to only siTDP-43-transfected cells, indicating improved DNA integrity (**Figure 3B**).

To further confirm the effects of PNKP complementation on DNA integrity, long-amplicon quantitative PCR (LA-qPCR) was performed targeting long-range genomic regions of two actively transcribed genes - DNA polymerase beta (POLB) and RNA polymerase II (RNAPII). Analysis demonstrated a significant recovery of DNA integrity as shown by increased PCR band intensity in PNKP-OE cells treated with siTDP-43 compared to siTDP-43 alone treatment. The long amplicon product levels were normalized to a short amplicon product level across the indicated groups (**Figure 3C**).

Our recent studies suggest that the efficient recruitment of the DNA break-sealing complex, XRCC4/ DNA Lig4, is compromised in the absence of functional nuclear TDP-43 (5, 10). The mechanism underlying this disruption, however, remained elusive. Given PNKP's critical role in processing damaged DNA termini at DSB sites to generate ligatable 3'-OH and 5'-P ends, we investigated whether loss of PNKP activity contributes to the impaired recruitment of Lig4 complexes to the DNA DSB sites. Proximity ligation assays (PLA) revealed a significant reduction in Lig4 interactions with γH2AX-marked DSB sites in nuclei of TDP-43 KD cells (**Figure 3D**). This deficiency was effectively rescued in PNKP-OE cells, suggesting that the restoration of PNKP activity enhances the recruitment of DNA Lig4 to genomic DSBs.

TDP-43 Associates with PNKP in the TC-NHEJ Complex and Integrity of Transcribed Genes is Impaired Under Pathological Conditions

Our previous study demonstrates the presence of a pre-formed TC-NHEJ complex involving PNKP and other DSB repair proteins in mammalian brain samples (32, 35). PNKP plays a crucial role in RNA-templated error-free TC-NHEJ repair, thereby protecting the transcribed genome (21, 32, 33). RNA-templated TC-NHEJ is compromised in PNKP-depleted cells. Since our results indicate that either TDP-43 depletion or mislocalization can disrupt PNKP activity, we assessed its association with the TC-NHEJ components in NE from ALS and age-matched control patients' cortical brain samples using PNKP co-immunoprecipitation (co-IP) assay, revealing PNKP's interaction with TDP-43, which was significantly compromised in ALS samples (**Figure 4A**), indicating TDP-43's potential involvement in the TC-NHEJ pathway to facilitate PNKP-mediated DNA DSB repair. We also observed concomitant decrease in the association of other TC-NHEJ proteins, such as Lig4 and PFKFB3 under pathological conditions (**Figure 4A**). This result was consistent with our previous finding showing disruption of the TC-NHEJ repair pathway in TDP-43 pathology.

Since PNKP is involved in preferential repair of the transcribed genome, we assessed genome damage in actively transcribed versus non-transcribed regions in genomic DNA from cortical tissues of ALS and FTD patients versus age-matched control tissues. Analysis revealed a significant increase in DSB accumulation in transcribed genes (Enolase and NeuroD) compared to non-transcribed genes (MyH2 and MyH4) in ALS-TDP-43 patient tissues (**Figure 4B**). This preferential accumulation of DNA damage in transcriptionally active regions was consistent with a decrease in PNKP activity and impaired TC-NHEJ repair in TDP-43 pathology.

Reduced PFKFB3 Levels Correlate with Loss of PNKP Activity in ALS/FTD and PNKP Activity is Restored by F2,6BP Supplementation

We have demonstrated that F2,6BP, the product of PFKFB3, is a positive co-regulator of PNKP activity *in vivo* (35). We further reported reduced levels of PFKFB3 and F2,6BP in the affected regions of HD and SCA3 patient brain samples - a plausible cause of PNKP inactivation in these pathologies. Therefore, to get further insight into mechanism of near complete loss of PNKP activity in ALS/FTD, we assessed levels of PFKFB3 and F2,6BP in patients versus age-matched healthy controls. IB analysis revealed a significant decrease in PFKFB3 levels in cortical samples from ALS and FTD patients compared to age-matched controls (**Figure 5A**; *Supplementary* **Figure S1B**). This result was consistent with observation of reduced PFKFB3 level associated with depletion of TDP-43 in HEK293 cells (**Figure 2A**). We further observed that levels of F2,6BP were significantly lower in ALS/FTD patient brain samples compared to age-matched controls (**Figure 5B**), correlating with the reduced levels of PFKFB3 in those samples. These data further suggest a potential link between disrupted glycolytic regulation and impaired DNA repair mechanisms under neurodegenerative conditions. Next, we tested the effect of exogenous F2,6BP supplementation in restoring nuclear PNKP activity in patient samples. Supplementation with F2,6BP significantly restored PNKP activity in the NE of ALS tissues (**Figure 5C**; Lns 7-10 vs. Lns 3-6). We further observed that F2,6BP restored PNKP activity in a dose-dependent manner both in sporadic ALS (**Figure 5D**, Lns 5-6) and Guam-ALS samples **(Figure 5E**, Lns 5-7**)** Notably, we found that only F2,6BP but not F1,6BP or F6P could stimulate PNKP activity, which was in agreement with our previous findings in polyQ diseases (35). These results also highlight that restoring F2,6BP levels can stabilize the PNKP activity, even under stress conditions, thus

indicating a metabolic reprograming-mediated novel regulatory pathway for restoring DNA DSB repair machinery and genome integrity in neurodegenerative diseases.

Characterization of Patient Cell Lines Reveals TDP-43 Pathology-Associated Abrogation of PNKP Activity and Its Subsequent Rescue by F2,6BP Supplementation

To elucidate the impact of ALS and FTD-associated TDP-43 mutations on DNA repair mechanisms, we utilized three ALS and one FTD patient-derived cell lines. Initially, we focused on two ALS-linked TDP-43 mutations G287S and G298S (schematic in **Figure 6A**) and an isogenic CRISPR/Cas9-mediated mutation corrected NPSC line for the G287S mutation (schematic in **Figure 6B**) to elucidate the mechanistic effect of these mutations on DNA DSB repair and PNKP activity. We first examined the subcellular localization of TDP-43 and its phosphorylated form S409/410 (pTDP-43). IF analysis revealed significant cytoplasmic mislocalization of TDP-43 G287S mutant compared to its isogenic TDP-43 S287G variant, which displayed predominantly nuclear TDP-43 (**Figure 6C**). Mander's coefficient of colocalization of total TDP-43 overlapping pTDP-43 and *vice versa* confirmed reduced colocalization of TDP-43 with pTDP-43 in the mutant cells compared to respective control cells, underscoring the nuclear clearance effect of G287S mutation on TDP-43 in ALS.

We next assessed DNA damage in these models by IF-based co-staining of TDP-43 and γH2AX, exhibiting a significant increase in γH2AX foci count in G287S mutant NPCs with higher signal intensities of cytosolic TDP-43 compared to the isogenic control cells, suggesting a correlation between TDP-43 mislocalization and genomic instability (**Figure 6D**).

Based on these characterizations, we next assessed PFKFB3 levels and 3′-phosphatase activity of PNKP in the G287S mutant vs. its isogenic line to correlate with our earlier results in ALS/FTD patient samples. IB analysis of these cells revealed a significant reduction (~60%) in PFKFB3 protein levels in G287S NPSCs relative to their isogenic controls, while PNKP protein levels remained unaffected (**Figure 6E**). In this line, marked decrease in PNKP activity was correlated with reduced PFKFB3 levels in these samples, and this loss of activity was restored in a dose-dependent manner by F2,6BP supplementation in vitro (**Figure 6F**). This further demonstrates that reduced PNKP activity is linked to decreased PFKFB3/F2,6BP levels under pathological conditions.

We extended our analysis to TDP-43 G298S mutant NPSCs derived from ALS patients. Similar to the G287S mutant, IF imaging showed cytosolic mislocalization and increased phosphorylation (S409/410) of TDP-43 G298S cells, compared to TDP-43 WT NPSCs, as measured by Mander's coefficient analysis (**Figure 6G**). IB analysis revealed a substantial elevation in γH2AX levels in G298S mutant, indicating elevated DNA damage, while total H2A.II levels remained comparable between mutant and WT cells (**Figure 6H**). Finally, we assessed PNKP activity in the G298S mutant cells. Similar to our findings with G287S, we observed an ~80% reduction in PNKP activity in G298S NPSCs compared to WT controls, while PNKP activity could be restored by F2,6BP in a dose-dependent manner (**Figure 6I**).

Further investigations extended to an engineered ALS-linked TDP-43 Q331K mutant and its isogenic control (*Supplementary* **Figure S2A**) revealed similar patterns of TDP-43 mislocalization-associated, increased phosphorylation (*Supplementary* **Figure S2B**), reduced PFKFB3 levels (*Supplementary* **Figure S2C**), and decreased PNKP activity (*Supplementary* **Figure SD**), compared to respective controls. In addition, we examined an FTD patient-derived cell line harboring both TDP-43 A282T and a C9ORF72 repeat expansion mutations (*Supplementary* **Figure S2E**) for PNKP activity and the effect of F2,6BP supplementation on FTD

iPSCs, which demonstrated a consistent result with other TDP-43 mutant cell lines (*Supplementary* **Figure S2F**), underscoring the therapeutic potential of F2,6BP in restoring DNA repair capacity in TDP-43 pathology.

Altered PNKP Activity and Its Restoration by F2,6BP in ALS-TDP-43 mouse model

Finally, we investigated the impact of TDP-43 pathology on PNKP level and activity in an ALS-TDP-43 mouse model (13). **Figure 7A** shows the schematic of the genetic construct employed to drive murine TDP-43ΔNLS mutant expression in these mice. We first analyzed the subcellular localization of TDP43 and its phosphorylated form, pTDP-43, in the cortex of both sham and ALS mice by IF (**Figure 7B**). Quantitative analysis using Mander's coefficient demonstrated a significant increase in colocalization of TDP-43 and pTDP-43 in ALS mice brains, emphasizing the pathological redistribution of TDP-43.

We next assessed the levels of PFKFB3 and PNKP in cortical samples from ALS and sham mice. IB analysis revealed a significant reduction in PFKFB3 protein levels in the NE of ALS mice compared to controls, while PNKP levels remained unaltered (**Figure 7C**). We further evaluated PNKP enzymatic function in NE of cortical tissues of ALS and age-matched sham mice (**Figure 7D**), which displayed markedly decreased PNKP activity in ALS mice brains (Lns 6-9) relative to sham controls (Lns 2-5). Importantly, we observed a dose-dependent increase in PNKP activity following F2,6BP supplementation, whereas the glycolytic metabolites F1,6BP and F6P did not produce similar effects (**Figure 7E**). Overall, these results indicate that TDP-43 pathology in ALS mice leads to significant reductions in PNKP activity. This effect could be correlated with reduced PFKFB3 levels, which was supported by our results that treatment with F2,6BP could effectively rescue PNKP function, suggesting a promising metabolic approach to restoring DNA repair mechanisms in ALS.

Our current study documents the intricate relationship between TDP-43, PNKP, and PFKFB3 in ALS and FTD, as shown schematically in **Figure 8**. By employing patient-derived cells, murine ALS-TDP-43 mouse model, and autopsied ALS and FTD brain tissues, we demonstrate that 3'-phosphatase activity of PNKP is significantly reduced in ALS and FTD, conditions marked by TDP-43 mutations and mislocalization. This decrease in PNKP activity could be attributed to degradation of PFKFB3 protein under ALS/FTD pathological conditions, and thereby subsequent decrease in the level of its product, F2,6BP, a positive co-factor of PNKP activity. These alterations correlate with the observed DNA damage accumulation in the transcribed genome, an observation consistent with our previous results in PNKP-depleted (21) and PFKFB3-depleted (35) mammalian cell models. Reduction in PNKP activity might lead to accumulation of "non-ligatable" 3´-Phosphate DNA ends, which may impair recruitment of XRCC4-Lig4 complex to the DSB sites (as depicted in **Figure 8**), a hallmark of TDP-43 pathology (5, 10, 13). Notably, our results indicate that supplementation with F2,6BP can restore PNKP activity and potentially mitigate genomic instability in neurodegenerative diseases. Overall, our findings suggest that the loss of PNKP activity in TDP-43-associated neurodegeneration is closely tied to disrupted metabolic regulation via PFKFB3. It has now been established that PFKFB3 is stabilized during brain excitation (45). Our results are therefore consistent as it shows that PFKFB3's level is low in the nucleus only under ALS/FTD pathogenic condition but not in post-mitotic healthy neurons. We hypothesize that locally produced F2,6BP is transferred directly to PNKP within the TC-NHEJ complex to potentiate 3´-phosphatase activity of PNKP under normal physiological conditions and this process is severely impaired under pathogenic conditions.

However, the mechanism of PFKFB3 degradation in NE from ALS/FTD patients, mice and patient-derived cells requires further investigation.

While advancements have been made in the treatment of ALS, particularly with the development of therapies targeting specific genetic mutations, FTD remains largely without effective disease-modifying treatments. Riluzole was the first drug approved for ALS therapy. It has been shown to extend patient survival by a few months, however, it did not show any benefit for patients with advanced ALS (46, 47). Another potent antioxidant Edaravone can also halt the disease progression only if given at the early stage of the disease (48, 49). Notably, the landscape of clinical trials targeting TDP-43 in ALS is dynamic, with a variety of therapeutic approaches under investigation (50-52). These efforts reflect a growing recognition of the need to address TDP-43 pathology, which is central to many ALS cases. Continued advancements in this area hold promise for developing effective treatments for ALS patients.

Finally, our study not only elucidates the molecular underpinnings of TDP-43 associated genomic instability but also suggests that targeting metabolic pathways could be a viable therapeutic strategy. By restoring PNKP function through F2,6BP supplementation, we provide a novel approach to counteract the DNA repair deficiencies observed in TDP-43 related neurodegeneration via modulating the glycolytic pathway, offering a new direction for therapeutic development aimed at enhancing the genome maintenance machinery in neurodegenerative conditions.

Supplementary Information

The online version contains supplementary materials, which includes supplementary Figs. S1-2 and Tables S1-2.

Acknowledgements

We thank Prof. Ian Robey at the Department of Veterans Affairs Biorepository and Prof. Ralph Garruto at Binghamton brain bank for providing the postmortem brain tissue specimens from ALS, Guam-ALS and FTD patients.

Funding

This research is supported by the National Institute of Neurological Disorders and Stroke of the National Institutes of Health (NIH-NINDS) funds under award numbers RF1NS112719 (M.L.H), R03AG064266 (M.L.H), R01 NS073976 (T. H), R56NS073976 (T. H.), R01AI163327 (G.G.) and R21 AG078635 (G.G).

Author contributions

M.L.H. and T.H. conceived and designed the project and edited the final manuscript. J.M. and A.C performed the majority of the experiments and wrote the manuscript, with crucial assistance from V.H.M., M.K., S.M.M, V.V., M.M. and G.G. All authors participated in data analyses and interpretation.

Data availability

All relevant data generated and analyzed in this study are available in this manuscript, online supplementary information or upon reasonable request.

Declarations

Conflict of interest
The authors declare no conflicts of interest.

Ethics Approval
The animal study protocol was approved by the Houston Methodist's Institutional Animal Care and Use Committee under the approval number ISO00006797.

References

1. Neumann M. et al. Ubiquitinated TDP-43 in frontotemporal lobar degeneration and amyotrophic lateral sclerosis. *Science* **314**(5796), 130-133 (2006).
2. Arai T. et al. TDP-43 is a component of ubiquitin-positive tau-negative inclusions in frontotemporal lobar degeneration and amyotrophic lateral sclerosis. *Biochem Biophys Res Commun* **351**(3), 602-611 (2006).
3. Geser F. et al. Pathological TDP-43 in parkinsonism-dementia complex and amyotrophic lateral sclerosis of Guam. *Acta Neuropathol* **115**(1), 133-145 (2008).
4. Feldman E. L. et al. Amyotrophic lateral sclerosis. *Lancet* **400**(10360), 1363-1380 (2022).
5. Mitra J. et al. Motor neuron disease-associated loss of nuclear TDP-43 is linked to DNA double-strand break repair defects. *Proc Natl Acad Sci U S A* **116**(10), 4696-4705 (2019).
6. Highley J. R. et al. Loss of nuclear TDP-43 in amyotrophic lateral sclerosis (ALS) causes altered expression of splicing machinery and widespread dysregulation of RNA splicing in motor neurones. *Neuropathol Appl Neurobiol* **40**(6), 670-685 (2014).
7. Mori F. et al. Colocalization of TDP-43 and stress granules at the early stage of TDP-43 aggregation in amyotrophic lateral sclerosis. *Brain Pathol* **34**(2), e13215 (2024).
8. Fang M. et al. Loss of TDP-43 function contributes to genomic instability in amyotrophic lateral sclerosis. *Front Neurosci* **17**, 1251228 (2023).
9. Konopka A. et al. Impaired NHEJ repair in amyotrophic lateral sclerosis is associated with TDP-43 mutations. *Mol Neurodegener* **15**(1), 51 (2020).
10. Guerrero E. N. et al. Amyotrophic lateral sclerosis-associated TDP-43 mutation Q331K prevents nuclear translocation of XRCC4-DNA ligase 4 complex and is linked to genome damage-mediated neuronal apoptosis. *Hum Mol Genet* **28**(15), 2459-2476 (2019).
11. Giannini M. et al. TDP-43 mutations link Amyotrophic Lateral Sclerosis with R-loop homeostasis and R loop-mediated DNA damage. *PLoS Genet* **16**(12), e1009260 (2020).
12. Hill S. J. et al. Two familial ALS proteins function in prevention/repair of transcription-associated DNA damage. *Proc Natl Acad Sci U S A* **113**(48), E7701-e7709 (2016).
13. Mitra J. et al. Endogenous TDP-43 mislocalization in a novel knock-in mouse model reveals DNA repair impairment, inflammation, and neuronal senescence. *Res Sq*, (2024).
14. Lopez-Gonzalez R. et al. Poly(GR) in C9ORF72-Related ALS/FTD Compromises Mitochondrial Function and Increases Oxidative Stress and DNA Damage in iPSC-Derived Motor Neurons. *Neuron* **92**(2), 383-391 (2016).
15. Kay J., Thadhani E., Samson L., Engelward B. Inflammation-induced DNA damage, mutations and cancer. *DNA Repair (Amst)* **83**, 102673 (2019).
16. Pálmai-Pallag T., Bachrati C. Z. Inflammation-induced DNA damage and damage-induced inflammation: a vicious cycle. *Microbes Infect* **16**(10), 822-832 (2014).

17. Kiraly O., Gong G., Olipitz W., Muthupalani S., Engelward B. P. Inflammation-induced cell proliferation potentiates DNA damage-induced mutations in vivo. *PLoS Genet* **11**(2), e1004901 (2015).
18. Lan L. et al. In situ analysis of repair processes for oxidative DNA damage in mammalian cells. *Proc Natl Acad Sci U S A* **101**(38), 13738-13743 (2004).
19. Jilani A. et al. Molecular cloning of the human gene, PNKP, encoding a polynucleotide kinase 3'-phosphatase and evidence for its role in repair of DNA strand breaks caused by oxidative damage. *J Biol Chem* **274**(34), 24176-24186 (1999).
20. Karimi-Busheri F. et al. Molecular characterization of a human DNA kinase. *J Biol Chem* **274**(34), 24187-24194 (1999).
21. Chakraborty A. et al. Classical non-homologous end-joining pathway utilizes nascent RNA for error-free double-strand break repair of transcribed genes. *Nat Commun* **7**, 13049 (2016).
22. Wiederhold L. et al. AP endonuclease-independent DNA base excision repair in human cells. *Mol Cell* **15**(2), 209-220 (2004).
23. Das A. et al. NEIL2-initiated, APE-independent repair of oxidized bases in DNA: Evidence for a repair complex in human cells. *DNA Repair (Amst)* **5**(12), 1439-1448 (2006).
24. Aceytuno R. D. et al. Structural and functional characterization of the PNKP-XRCC4-LigIV DNA repair complex. *Nucleic Acids Res* **45**(10), 6238-6251 (2017).
25. Shen J. et al. Mutations in PNKP cause microcephaly, seizures and defects in DNA repair. *Nat Genet* **42**(3), 245-249 (2010).
26. Poulton C. et al. Progressive cerebellar atrophy and polyneuropathy: expanding the spectrum of PNKP mutations. *Neurogenetics* **14**(1), 43-51 (2013).
27. Bras J. et al. Mutations in PNKP cause recessive ataxia with oculomotor apraxia type 4. *Am J Hum Genet* **96**(3), 474-479 (2015).
28. Shimada M., Dumitrache L. C., Russell H. R., McKinnon P. J. Polynucleotide kinase-phosphatase enables neurogenesis via multiple DNA repair pathways to maintain genome stability. *Embo j* **34**(19), 2465-2480 (2015).
29. Islam A. et al. Functional analysis of a conserved site mutation in the DNA end processing enzyme PNKP leading to ataxia with oculomotor apraxia type 4 in humans. *J Biol Chem* **299**(5), 104714 (2023).
30. Dumitrache L. C., McKinnon P. J. Polynucleotide kinase-phosphatase (PNKP) mutations and neurologic disease. *Mech Ageing Dev* **161**(Pt A), 121-129 (2017).
31. Gao R. et al. Mutant huntingtin impairs PNKP and ATXN3, disrupting DNA repair and transcription. *Elife* **8**, (2019).
32. Chakraborty A. et al. Deficiency in classical nonhomologous end-joining-mediated repair of transcribed genes is linked to SCA3 pathogenesis. *Proc Natl Acad Sci U S A* **117**(14), 8154-8165 (2020).
33. Chakraborty A. et al. Human DNA polymerase η promotes RNA-templated error-free repair of DNA double-strand breaks. *J Biol Chem* **299**(3), 102991 (2023).
34. Welsh J. A. et al. Minimal information for studies of extracellular vesicles (MISEV2023): From basic to advanced approaches. *J Extracell Vesicles* **13**(2), e12404 (2024).
35. Chakraborty A. et al. Fructose-2,6-bisphosphate restores DNA repair activity of PNKP and ameliorates neurodegenerative symptoms in Huntington's disease. *Proc Natl Acad Sci U S A* **121**(39), e2406308121 (2024).

36. Moretton A., Loizou J. I. Interplay between Cellular Metabolism and the DNA Damage Response in Cancer. *Cancers (Basel)* **12**(8), (2020).
37. Ros S., Schulze A. Balancing glycolytic flux: the role of 6-phosphofructo-2-kinase/fructose 2,6-bisphosphatases in cancer metabolism. *Cancer Metab* **1**(1), 8 (2013).
38. Yalcin A. et al. Nuclear targeting of 6-phosphofructo-2-kinase (PFKFB3) increases proliferation via cyclin-dependent kinases. *J Biol Chem* **284**(36), 24223-24232 (2009).
39. Gustafsson N. M. S. et al. Targeting PFKFB3 radiosensitizes cancer cells and suppresses homologous recombination. *Nat Commun* **9**(1), 3872 (2018).
40. Chakraborty A. et al. F2,6BP restores mitochondrial genome integrity in Huntington's Disease. *bioRxiv*, 2024.2011.2004.621834 (2024).
41. Fazal R. et al. HDAC6 inhibition restores TDP-43 pathology and axonal transport defects in human motor neurons with TARDBP mutations. *Embo j* **40**(7), e106177 (2021).
42. Smith A. S. T. et al. Human Induced Pluripotent Stem Cell-Derived TDP-43 Mutant Neurons Exhibit Consistent Functional Phenotypes Across Multiple Gene Edited Lines Despite Transcriptomic and Splicing Discrepancies. *Front Cell Dev Biol* **9**, 728707 (2021).
43. Kodavati M. et al. FUS unveiled in mitochondrial DNA repair and targeted ligase-1 expression rescues repair-defects in FUS-linked motor neuron disease. *Nat Commun* **15**(1), 2156 (2024).
44. Wang H. et al. Mutant FUS causes DNA ligation defects to inhibit oxidative damage repair in Amyotrophic Lateral Sclerosis. *Nat Commun* **9**(1), 3683 (2018).
45. Díaz-García C. M. et al. Neuronal Stimulation Triggers Neuronal Glycolysis and Not Lactate Uptake. *Cell Metab* **26**(2), 361-374.e364 (2017).
46. Saitoh Y., Takahashi Y. Riluzole for the treatment of amyotrophic lateral sclerosis. *Neurodegener Dis Manag* **10**(6), 343-355 (2020).
47. Petrov D., Mansfield C., Moussy A., Hermine O. ALS Clinical Trials Review: 20 Years of Failure. Are We Any Closer to Registering a New Treatment? *Front Aging Neurosci* **9**, 68 (2017).
48. Cho H., Shukla S. Role of Edaravone as a Treatment Option for Patients with Amyotrophic Lateral Sclerosis. *Pharmaceuticals (Basel)* **14**(1), (2020).
49. Brooks B. R. et al. Intravenous edaravone treatment in ALS and survival: An exploratory, retrospective, administrative claims analysis. *EClinicalMedicine* **52**, 101590 (2022).
50. Khamaysa M., Pradat P. F. Status of ALS Treatment, Insights into Therapeutic Challenges and Dilemmas. *J Pers Med* **12**(10), (2022).
51. Afroz T. et al. Immunotherapy targeting the C-terminal domain of TDP-43 decreases neuropathology and confers neuroprotection in mouse models of ALS/FTD. *Neurobiol Dis* **179**, 106050 (2023).
52. Fang M. Y. et al. Small-Molecule Modulation of TDP-43 Recruitment to Stress Granules Prevents Persistent TDP-43 Accumulation in ALS/FTD. *Neuron* **103**(5), 802-819.e811 (2019).

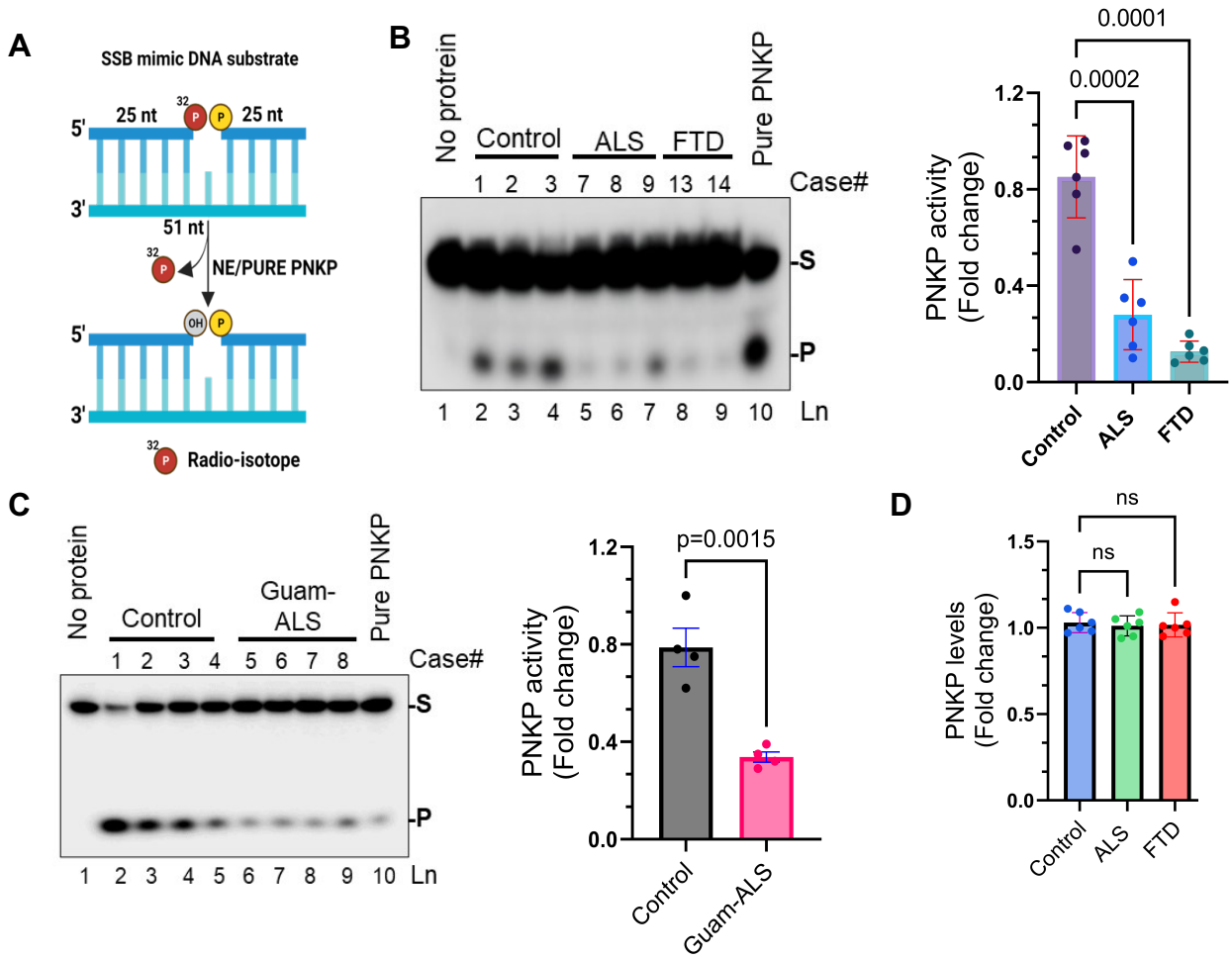

Figure 1. PNKP activity is significantly diminished in sporadic ALS and FTD patient tissues with TDP-43-positive inclusions.

A) Schematic representation of radio-labeled ^{32}P release by 3'-phosphatase activity of PNKP on a duplex oligonucleotide substrate simulating a DNA single-strand break (SSB).

B) Representative image demonstrating reduced PNKP activity in the nuclear extracts (NE) of ALS-TDP-43 (Lns 5-7) and FTD-TDP-43 (Lns 8-9) cortical tissues compared to age-matched non-neurological controls (Lns 2-4). Ln 1: substrate only (negative control); Ln 10: purified PNKP (25 fmol) as positive control. The histogram displays quantification of PNKP activity as fold change, analyzed by two-way ANOVA. S: substrate, P: released phosphate.

C) PNKP activity assay from Guamanian ALS patient brain samples (Lns 6-9) compared to age-matched Guam controls (Lns 2-5). Quantification of PNKP activity as fold change was analyzed using a Student's t-test.

D) Quantitative histogram showing relative PNKP levels in patient brain specimens analyzed in B and C. Data analyzed using a Student's t-test.

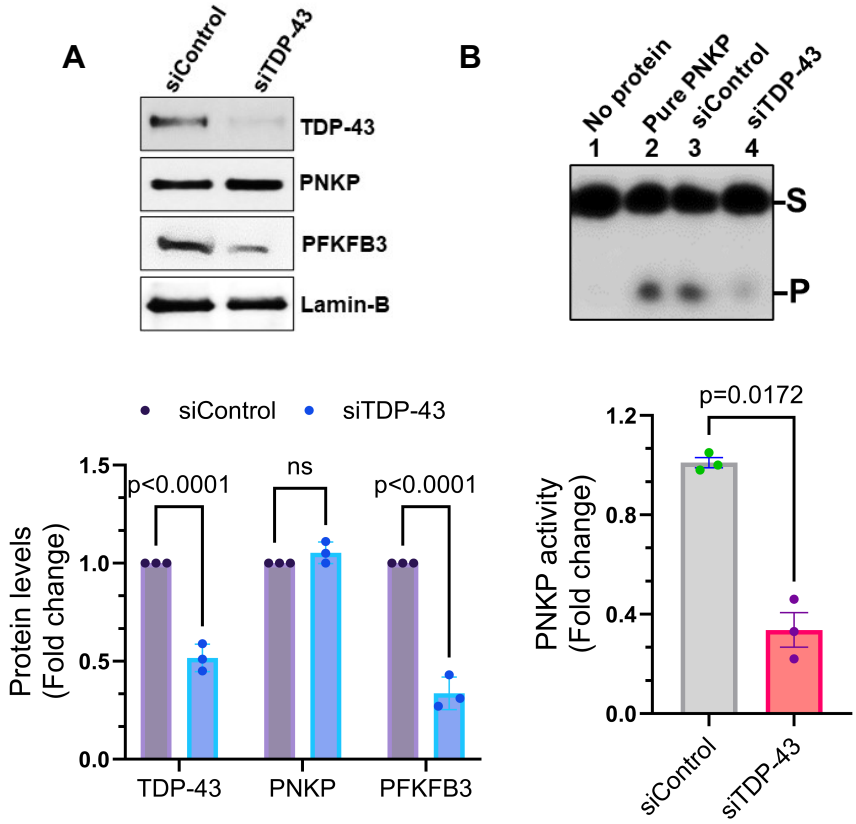

Figure 2. Loss of TDP-43 abolishes PNKP activity in cultured cells.
A) IB analysis showing levels of TDP-43, PNKP, and PFKFB3 in HEK293 cells treated with siTDP-43 or siControl. Lamin-B served as the nuclear loading control. The histogram shows quantification of protein levels as fold change, analyzed using two-way ANOVA.
B) Representative image of 3'-phosphatase activity of PNKP in the nuclear extracts of HEK293 cells transfected with siControl (Ln 3) or siTDP-43 (Ln 4). Ln 1: substrate alone; Ln 2: purified PNKP (25 fmol) as controls. Quantification of PNKP activity is presented as fold change. data were analyzed using a Student's t-test.

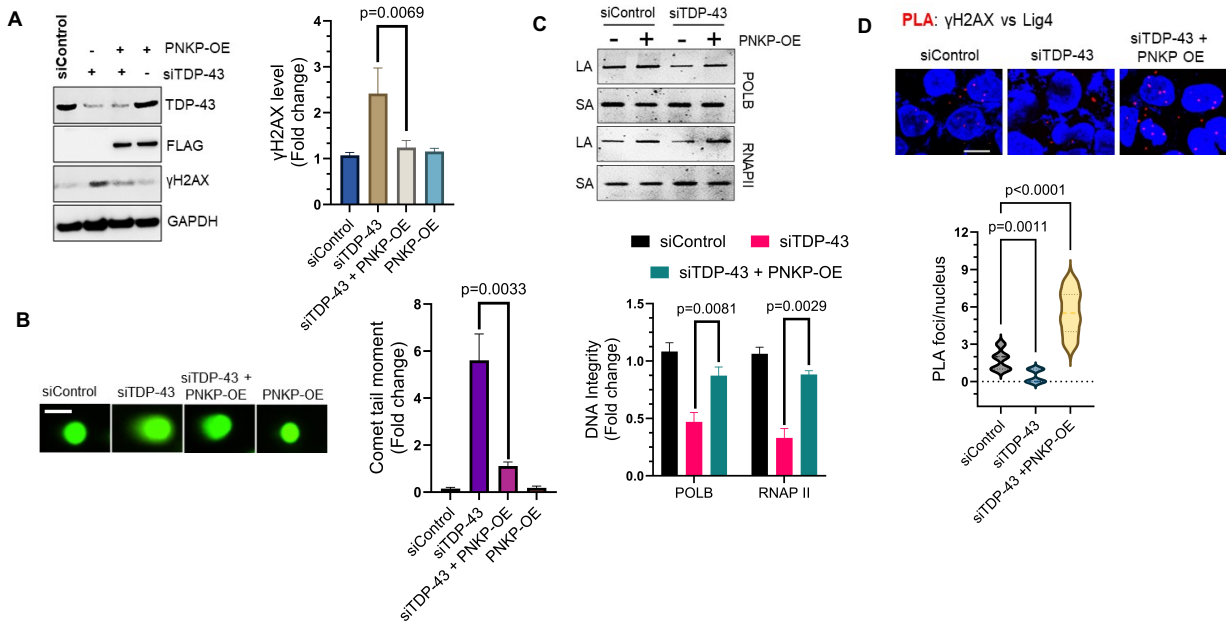

Figure 3. PNKP supplementation rescues DNA damage in TDP-43 KD cells. A. IB showing γH2AX levels in TDP-43 KD (siTDP-43) HEK293 cells with or without PNKP overexpression (OE). Histogram shows quantitation of γH2AX levels (band intensity, normalized to GAPDH). **B**. Neutral comet assay and quantitation of tail moment. N = 50 cells. Scale bar, 10 μm. **C**. DNA integrity analysis using LA-qPCR of POLB and RNAPII genomic regions. Quantitation of PCR products was performed using Pico-Green method in a plate reader. The long amplicon (10-12kb) was normalized to a short amplicon (~200bp) of the POLB and RNAPII genes and represented in the bar diagram as fold change of DNA integrity. **D**. PLA of Lig4 vs γH2AX, shows reduced signal in TDP-43 KD HEK293 cells, which was rescued after PNKP OE. Scale bar, 10 μm. Histogram shows quantitation of number of PLA foci per nuclei counted from 25 cells.

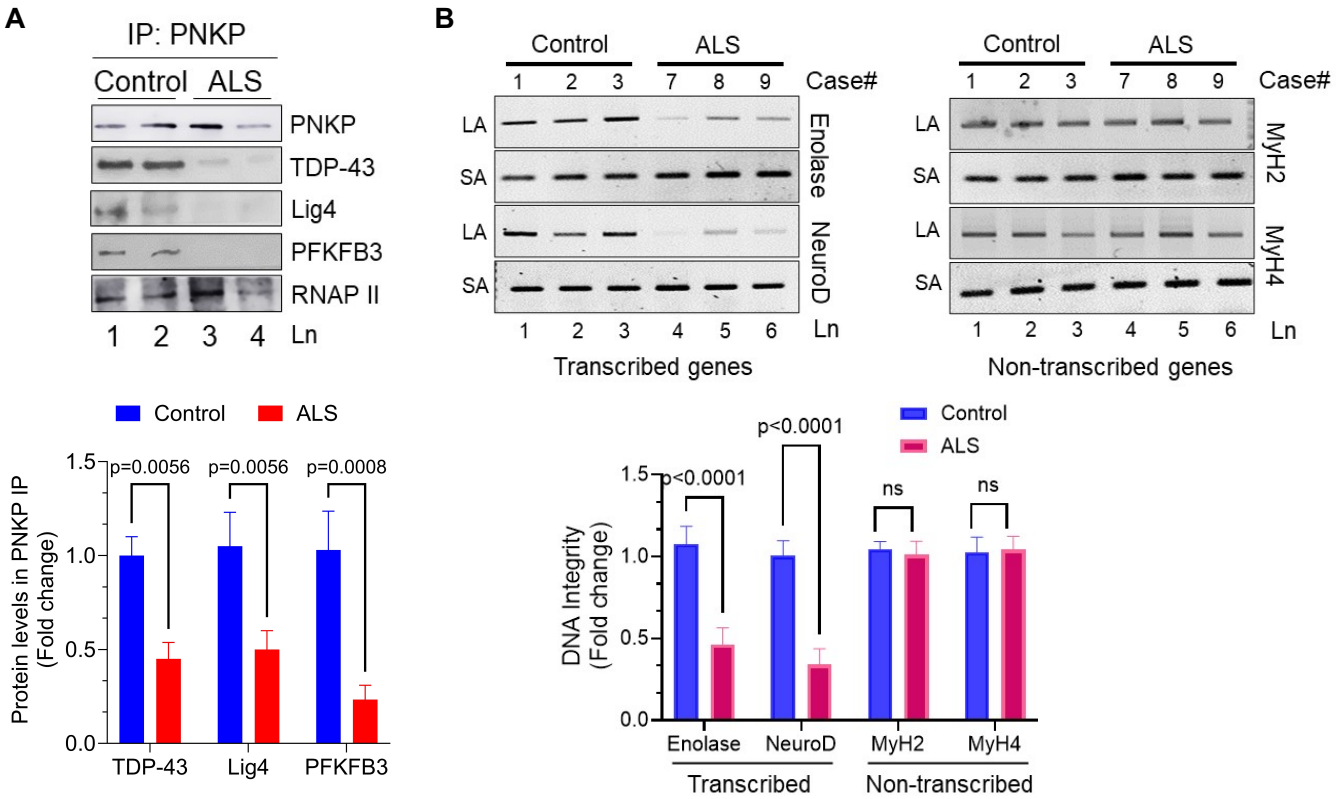

Figure 4. Partial characterization of the TC-NHEJ complex in post-mortem patient tissues and preferential accumulation of genome damage at transcribed genes in TDP-43 pathology. **A**. Nuclear extracts (NE) of human post-mortem brain (frontal cortex) (healthy control and ALS) were IP'd with anti-PNKP antibody and tested for associated proteins (as indicated). Quantitation of IP'd protein levels in terms of relative band intensity. **B**. Representative agarose gel images showing accumulation of genome damage in transcribed (Enolase & NeuroD) vs. non-transcribed (MyH2 & MyH4) genes in autopsied brain samples of control and ALS-TDP-43 patients (N=3) by LA-qPCR. The PCR products were independently quantified using a highly sensitive Pico-Green based method in a plate reader. Relative long amplicon values were normalized to short amplicon (~200bp) of the respective gene and represented in histogram as fold change of DNA integrity. ns=non-significant (p>0.05).

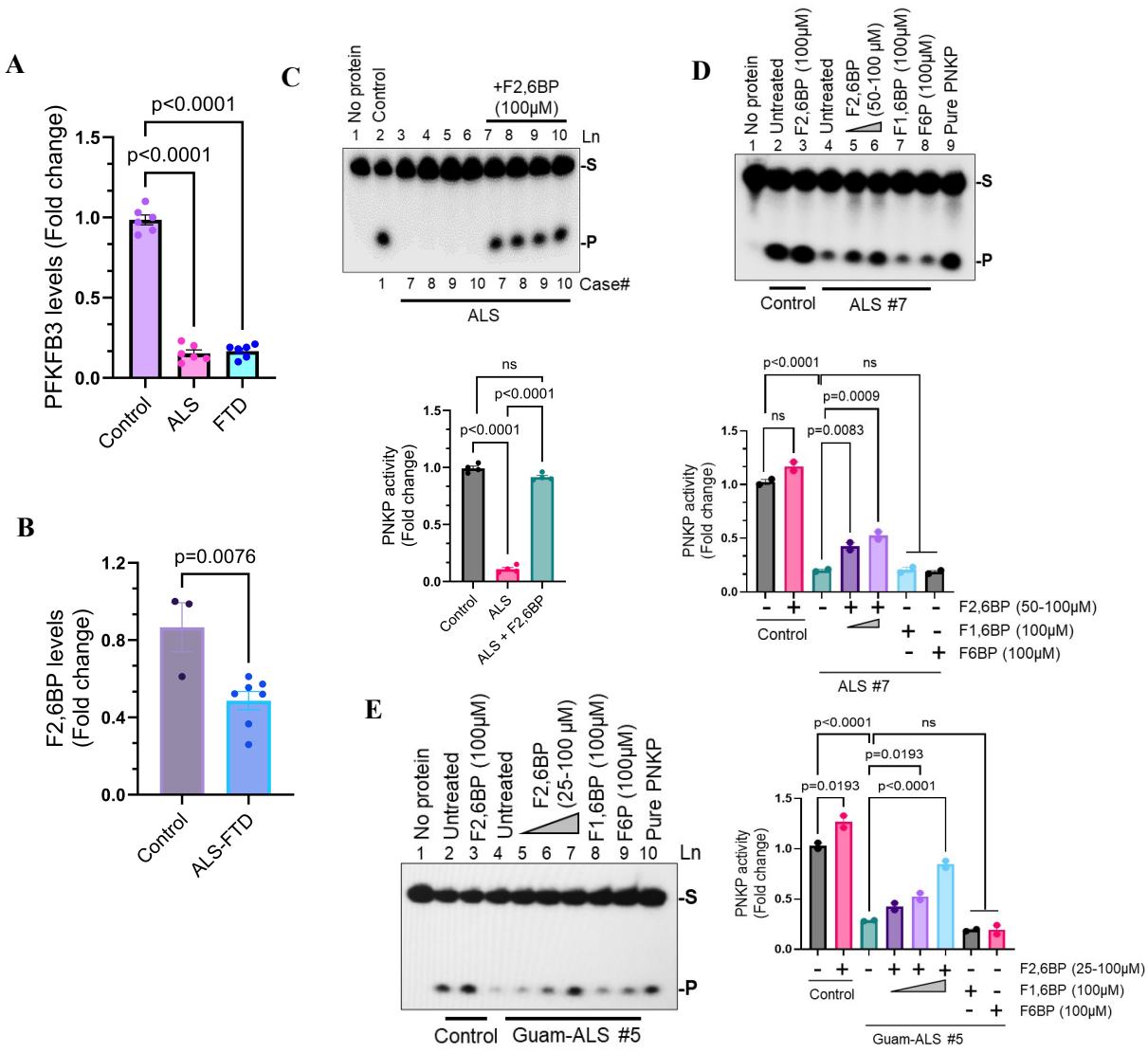

Figure 5. Reduced PFKFB3 and F2,6BP levels in ALS/FTD brains and restoration of PNKP activity by F2,6BP supplementation.

A) The bar graph illustrates relative levels of PFKFB3 normalized with HDAC2. Data were analyzed using one-way ANOVA.

B) Quantitation of F2,6BP levels in control (N=3), ALS (N=3) and FTD (N=4) patient frontal cortices.

C) Representative images showing 3'-phosphatase activity of PNKP in NE from ALS-TDP-43 samples (Lns 3-6) compared to age-matched non-neurological controls (Ln 2), with activity restored upon adding the F2,6BP metabolite (Lns 7-10). Lane 1 shows the substrate-only negative control. The histogram quantifies PNKP activity as fold change, analyzed by one-way ANOVA. S: substrate, P: released phosphate.

D Representative image showing the concentration-dependent rescue of PNKP activity (Lns 5-6) by F2,6BP in a sporadic ALS-TDP-43 sample (Ln 4), compared with an age-matched control (Ln 2). F1,6BP and F6P were used as negative controls (Lns 7, 8). Lane 1 shows the substrate-only, lane 10: purified PNKP (25 fmol). The histogram presents relative PNKP activity as fold change, with analysis by two-way ANOVA.

E) Representative image demonstrating concentration-dependent restoration of PNKP activity by F2,6BP in a Guam-ALS-TDP-43 sample compared to an age-matched control, with F1,6BP and F6P serving as negative controls. The histogram represents relative PNKP activities as fold changes, analyzed via two-way ANOVA.

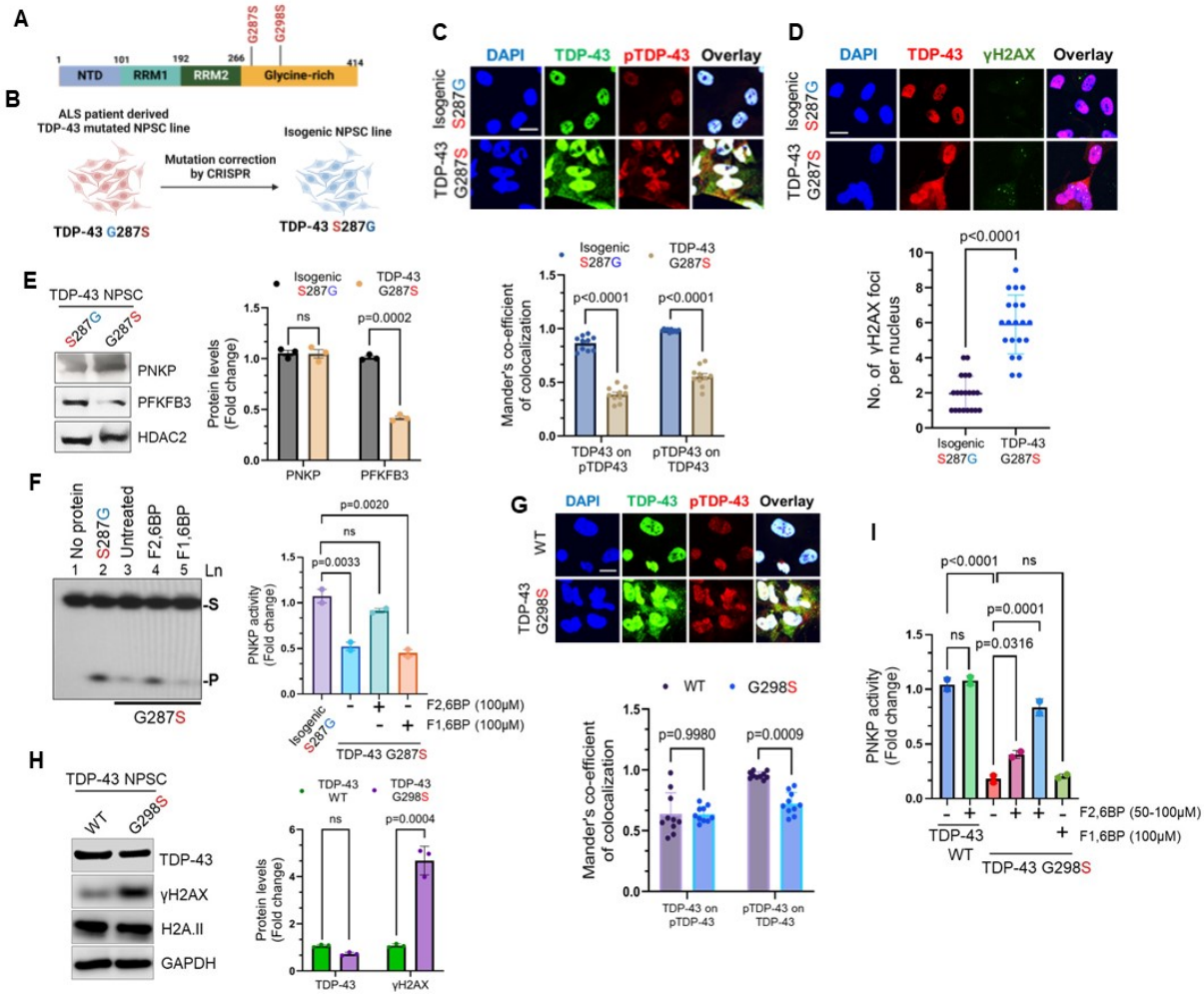

Figure 6. DNA Damage Induced by Mutant TDP-43 via PNKP Inhibition is Rescued by F2,6BP in ALS Patient Cell Lines.

A) Schematic representation of TDP-43 protein domains highlighting the G287S and G298S mutations.

B) CRISPR/Cas9-mediated correction of the G287S mutation to generate an isogenic S287G iPSC line, as schematically illustrated.

C) IF analysis of G287S mutant and isogenic S287G NPCs, showing cytosolic mislocalization of TDP-43 and its phosphorylated p409/410 form in the mutant cells. Mander's coefficient analysis quantifies colocalization between TDP-43 and pTDP-43, presented in the histogram.

D) IF imaging reveals γH2AX foci in G287S mutant NPCs but not in isogenic S287G cells. The histogram shows the average number of γH2AX foci per cell (N=25).

E) (Left) IB analysis of G287S mutant and isogenic S287G NPCs, demonstrating significantly reduced PFKFB3 protein levels) in mutant cells, while PNKP levels remain unchanged. HDAC2: Nuclear loading control. (Right) Quantification of relative levels of PFKFB3 and PNKP.

F) (left) Representative image displaying reduced PNKP activity in nuclear extracts from G287S mutant (Ln 3) and isogenic S287G NPCs (Ln 2) and its rescue by F2,6BP (Ln 4) but not F1,6BP (Ln 5). (right) Quantification in the histogram indicates reduction in PNKP activity in mutant cells (N=3). S: substrate, P: released phosphate. Lane 1, no protein.

G) IF analysis of G298S mutant NPCs derived from ALS patients reveals cytosolic mislocalization and the presence of phosphorylated (p409/410) TDP-43. Wild-type (WT) TDP-43 NPCs are used as controls. Mander's coefficient analysis quantifies WT and pTDP-43 localization, presented in the histogram.

H) IB analysis of WT and G298S mutant cell extracts showing increased γH2AX levels in mutant cells, with comparable total TDP-43 levels. H2A.II and GAPDH serve as controls. Quantification of band intensities from three independent experiments is shown in the histogram.

I) Quantitation of PNKP activity in nuclear extracts from G298S mutant and WT NPCs, with or without F2,6BP. The histogram quantifies reduction in PNKP activity in mutant cells

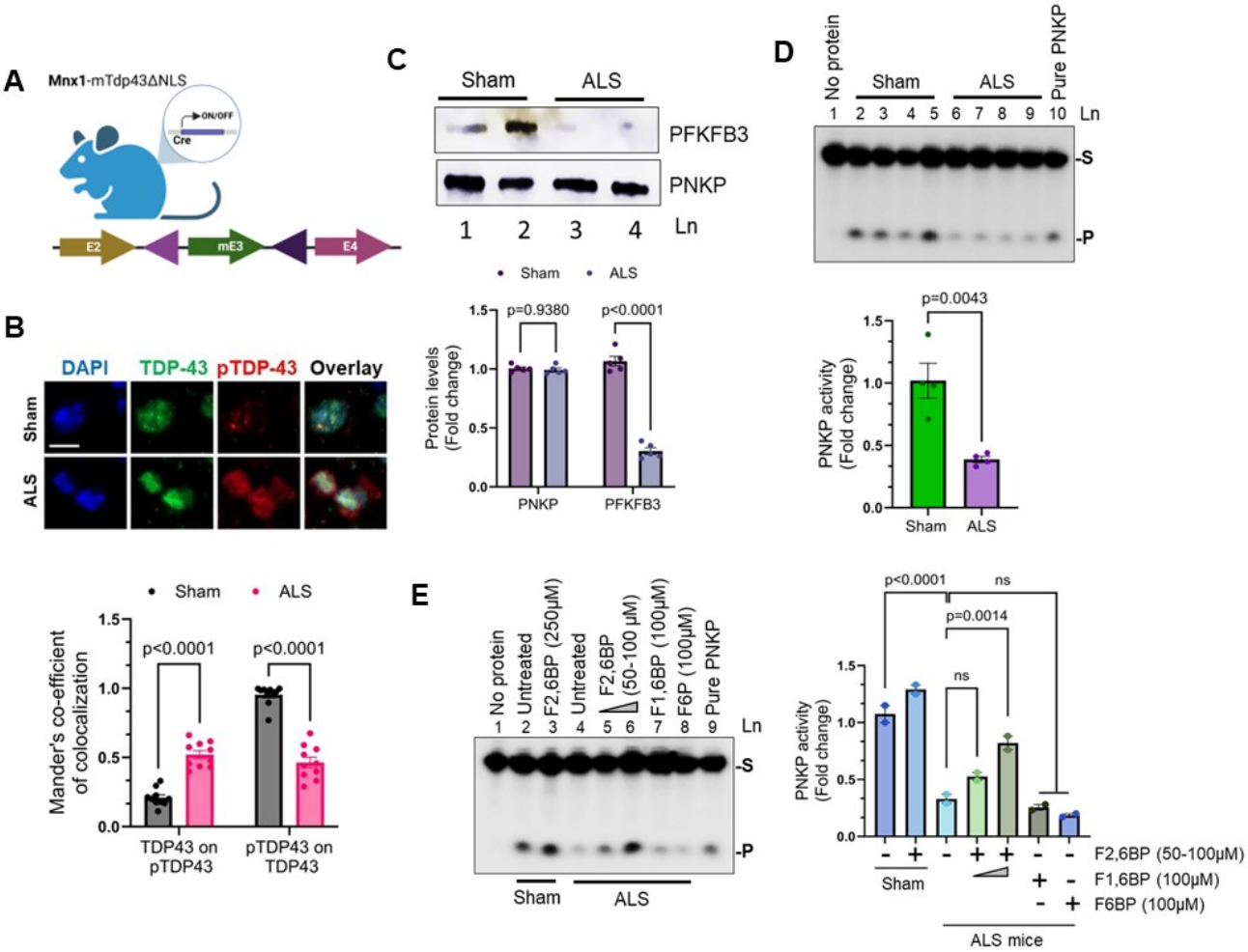

Figure 7. Reduced PNKP activity in TDP-43 mouse brain tissues correlates with PFKFB3 levels and its restoration by F2,6BP.

A) Schematic of the construct used to generate Tdp43-ΔNLS expression under the UBC promoter in C57BL6 mice. **B)** Representative IF images displaying subcellular distributions and colocalization of murine TDP-43 and its phosphorylated form (pTDP-43) in the cortex of sham and Mnx1-Cre::TDP-43ΔNLS mice. Nuclei were counterstained with DAPI. Scale bar, 10μm. Quantitation of TDP-43 fluorescence signal overlapping pTDP-43 and vice versa and expressed as Mander's coefficient. N=10 different fields/group. Data are analyzed by two-way ANOVA.

C) Representative IB images showing PNKP and PFKFB3 levels in sham and ALS cortical samples. Bar graph displaying changes in PNKP and PFKFB3 levels across the groups as fold changes. Data are analyzed by one-way ANOVA.

D) Representative image demonstrating reduced PNKP activity in the nuclear extracts of ALS (Lns 6-9) compared to age-matched sham controls (Lns 2-5). Ln 1: substrate only (negative control); Ln 10: substrate plus pure PNKP protein as positive control. The histogram displays the quantification of PNKP activity as fold change, analyzed by Student's t-test. S: substrate, P: released phosphate.

E) Representative image showing the rescue of PNKP activity by F2,6BP in a dose-dependent manner in ALS mice sample compared to WT, where F1,6BP and F6P served as negative controls. Histogram indicating relative PNKP activities as fold change across the groups. Data are analyzed by two-way ANOVA.

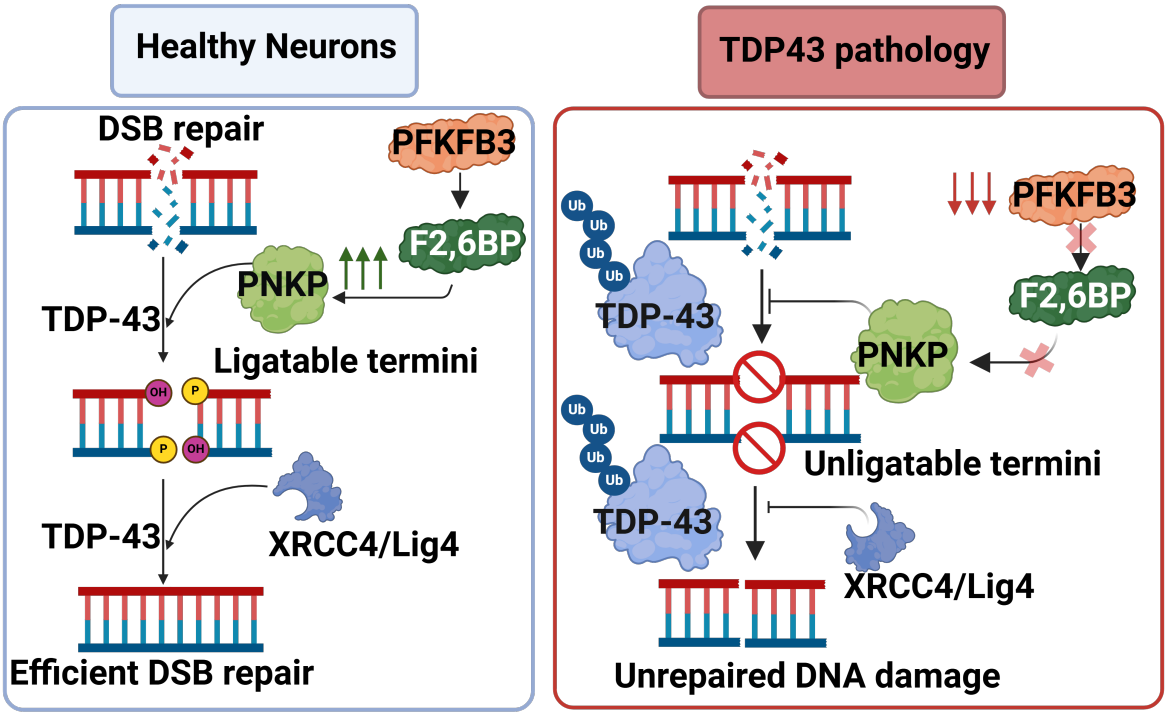

Figure 8. A Schematic Overview of PNKP Inhibition in Neurodegenerative Diseases with TDP-43 Pathology. The interaction between the glycolytic enzyme PFKFB3 and its product, the small molecule metabolite F2,6BP, plays a pivotal role in regulating PNKP activity and in turn for the repair of genome damage via transcription-coupled NHEJ. TDP-43 pathology results in reduced levels of PFKFB3 and significant loss of PNKP activity that results in neuronal loss. Supplementation of F2,6BP restores PNKP activity, suggesting its therapeutic potential.

Supplementary Material

Fructose-2,6-bisphosphate restores TDP-43 pathology-driven genome repair deficiency in motor neuron diseases

Joy Mitra[a,†], Anirban Chakraborty[c,†], Vikas H. Malojirao[a], Manohar Kodavati[a], Santi M. Mandal[d], Velmarini Vasquez[a], Mikita Mankevich[d], Gourisankar Ghosh[d], Muralidhar L. Hegde[a,b,*], Tapas Hazra[c,*].

[a]Division of DNA Repair Research, Center for Neuroregeneration, Department of Neurosurgery, Houston Methodist Research Institute, Houston, TX 77030, USA
[b]Department of Neuroscience, Weill Cornell Medical College, New York, NY 10065, USA
[c]Department of Internal Medicine, University of Texas Medical Branch, Galveston, TX, 77555, USA
[d]Department of Chemistry and Biochemistry, University of California San Diego, LA Jolla, California 92093, USA

† These authors contributed equally.

*Address of corresponding authors:

Muralidhar L Hegde, PhD
Professor, Center for Neuroregeneration
Department of Neurosurgery
Houston Methodist Research Institute, Houston, Texas 77030, USA
Tel: (713) 441-7456
E-mail: mlhegde@houstonmethodist.org

Tapas Hazra, PhD
Professor, Department of Internal Medicine-Pulmonary, Critical Care & Sleep Medicine
University of Texas Medical Branch, Galveston, TX 77555, USA
Tel: (409) 772-6308
Fax: (409) 747-8608
E-mail: tkhazra@utmb.edu

Supplementary Material includes two Tables and two Figures.

Supplementary Table S1: Demographic and clinical characteristics of ALS and FTD-TDP-43 patients and age-matched non-neurological control subjects. The TDP-43 inclusion status, provided by the sourcing biorepositories and independently validated by us, is indicated.

ID#	Age	Ethnicity	Sex	Pathology	Disease	TDP-43 pathology?
Cohort 1						
1	66	Hisp/Latino	M	Bronchopneumonia	Non-neurological	No
2	81	White	F	Diffuse Alveolar Damage; Sepsis; acute Colitis	Selective neuronal necrosis	No
3	62	Hisp/Latino	M	Cardiopulmonary dysfunction; Hypertensive cardiomyopathy	Non-neurological	No
4	68	Whie	M	Bronchopneumonia and pleuritis; T-cell lymphoma; Renal dysfunction.	Non-neurological	No
5	71	White	F	Myocardial Ischemia; Aortic stenosis.	Non-neurological	No
6	82	Hisp/Latino	M	Cardiac ischemia	Non-neurological	No
7	76	White	M	Respiratory insufficiency; TDP-43 Inclusions; NFT; Braak II; Spinal degeneration.	Rapid onset ALS	Yes
8	62	African/Am	M	Spinal degeneration; Arteriosclerosis; TDP-43 Inclusions	ALS & Heart failure	Yes
9	50	White	M	Spinal degeneration; Midbrain degeneration; TDP-43 skein-like inclusions.	ALS & Respiratory failure	Yes
10	80	White	M	Spinal degeneration; NFT; Lewy body; Arteriosclerosis; Braak IV/VI.	ALS & Intercostal Respiratory failure	Yes
11	58	White	F	Spinal degeneration; Lewy bodies in olfactory bulb; vascular disease.	ALS	Yes
12	83	African/Am	M	Spinal degeneration; Braak III/VI; NFT; Vascular disease	ALS	Yes
13	73	White	M	FTLD-TDP-43 inclusions with MND; Vascular disease.	FTD	Yes
14	78	White	M	TDP-43 and ubiquitin-positive inclusions in frontal, temporal, caudate and spinal cord; Degeneration of lateral and ventral cortico-spinal tract; Alzheimer's Braak III.	FTD	Yes
15	43	White	M	TDP-43-positive neurites; Neuronal loss; Purkinje loss; Spinal degeneration	FTD	Yes
16	86	White	M	Degeneration of lateral cortico-spinal tracts and ventral roots; loss of anterior horn cells in spinal cord; TDP-43-positive neurites in hippocampus, midbrain and frontal cortex.	FTD	Yes
17	79	Asian	M	MND; FTLD-TDP-43; atypical CTE with prominent subcortical and subcerebellar white matter degeneration; Alzheimer's Braak II/VI	FTD & Respiratory failure	Yes
18	53	Hisp/Latino	M	FTLD-TDP-43 with MND; Spinal degeneration.	FTD & Respiratory failure	Yes

Cohort 2: Guamanian Samples						
1	57	Guam	F	No NFT	Non-neurological	No
2	43	Guam	F	No NFT	Non-neurological	No
3	48	Guam	M	Anoxic encephalopathy; Cardiac arrhythmia.	Focal acute myocardial infarction.	No
4	49	Guam	M	Probable corona insufficiency	Non-neurological	No
5	45	Guam	M	Muscle atrophy; Bulbar palsy; Dysarthria; Dysphagia; No dementia.	Guamanian-ALS	Yes
6	34	Guam	F	Muscle atrophy; Bulbar palsy	Guamanian-ALS	Yes
7	54	Guam	F	Marked atrophy of facial, messeter and temporal muscles; Respiratory dysfunction; Fixed palate and increased Jaw Jerk.	Guamanian-ALS	Yes
8	47	Guam	F	Bular atrophy; Spinal spasticity; Muscle atrophy	Guamanian-ALS	Yes

Supplementary Table S2: List of oligonucleotides used in this study.

Primers	**Gene**	**Nucleotide sequence 5′ - 3′**	**Purpose**
TV140-F	POLB	AGTGGGCTGGATGTAACCTG	SA-PCR
TV141-R	POLB	CCAGTAGATGTGCTGCCAGA	SA-PCR
TV161-F	POLB	CATGTCACCACTGGACTCTGC AC	LA-qPCR
TV162-R	POLB	CCTGGAGTAGGAACAAAAATT GCT	LA-qPCR
TV21 RPmix	NeuroD (Human)	RealTimePrimers.com	SA-PCR and qRT-PCR
H-NeuroD1-LA-F	NeuroD (human)	CCGCGCTTAGCATCACTAAC	LA-qPCR
H-NeuroD1-LA-R	NeuroD (human)	TGGCACTGGTTCTGTGGTATT	LA-qPCR
H-ENO2-LA-F	Enolase (human)	ACGTGTGCTGCAAGCAATTT	LA-qPCR
H-ENO2-LA-R	Enolase (human)	CCTGAAACTCCCCTGACACC	LA-qPCR
H-MyH2-LA-F	MyH2 (human)	AAAGCCTGCCAAGCCCTAAA	LA-qPCR
H-MyH2-LA-R	MyH2 (human)	TGGTCAGCATGGCAAGTGAA	LA-qPCR
H-MyH4-LA-F	MyH4 (human)	CAGGAGTGGTCCCTAAAGGC	LA-qPCR
H-MyH4-LA-R	MyH4 (human)	GTAAAAACACGGTCCCTGCC	LA-qPCR
H-Enolase Primer mix	Enolase (human)	RealTimePrimers.com	SA-PCR
H-MyH2 Primer mix	MyH2 (human)	RealTimePrimers.com	SA-PCR
H-MyH4 Primer mix	MyH4 (human)	RealTimePrimers.com	SA-PCR

POLR2A LA FP	POLR2A (RNAP II)	CCTGTCCACTAGCTACCCCT	LA-qPCR (11.6 kb)
POLR2A LA RP	POLR2A (RNAP II)	CCCCTCCCCCTAACAGATCA	LA-qPCR (11.6 kb)
POLR2A SA FP	POLR2A (RNAP II)	GCTGGGATCGTGAACGGTAG	SA-PCR/DNA-qPCR (0.295kb)
POLR2A SA RP	POLR2A (RNAP II)	ATGGCGACAACTCACCTGG	SA-PCR/DNA-qPCR (0.295kb)

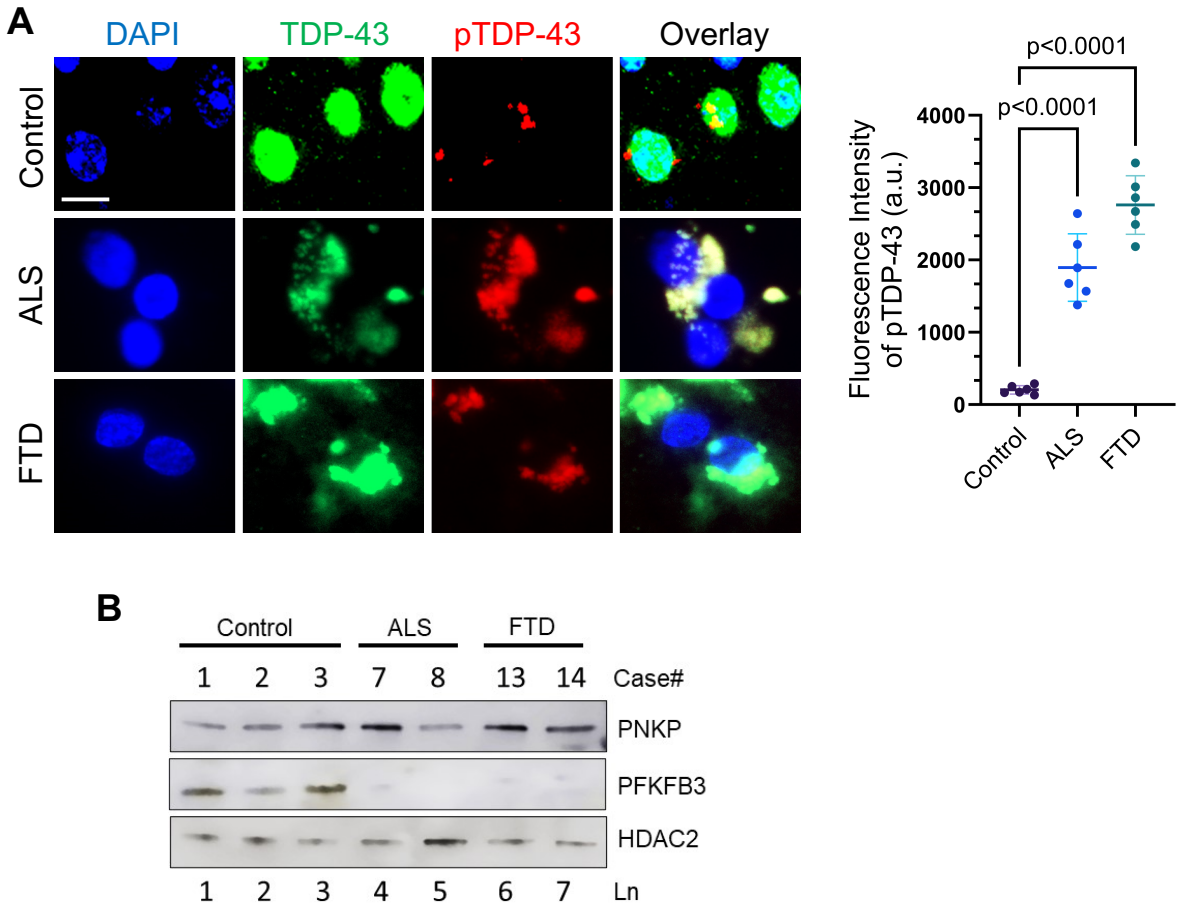

Supplementary Figure S1 (Related to Figure 1). Characterization of ALS/FTD patient brain tissue.

A) Representative immunofluorescence (IF) images showing cytosolic mislocalization of total TDP-43 and corresponding phosphorylated TDP-43 (pTDP-43, S409/410) expression levels in autopsied cortical sections from ALS, FTD, and age-matched non-neurological control samples (N = 6 cases per group). Scale bar, 10 µm. Quantification of fluorescence intensity (arbitrary units; a.u.) of pTDP-43 levels is included.

B) Representative IB image exhibiting PNKP and PFKFB3 levels in cortical samples from controls, ALS, and FTD patients, with HDAC2 as a loading control for nuclear extracts.

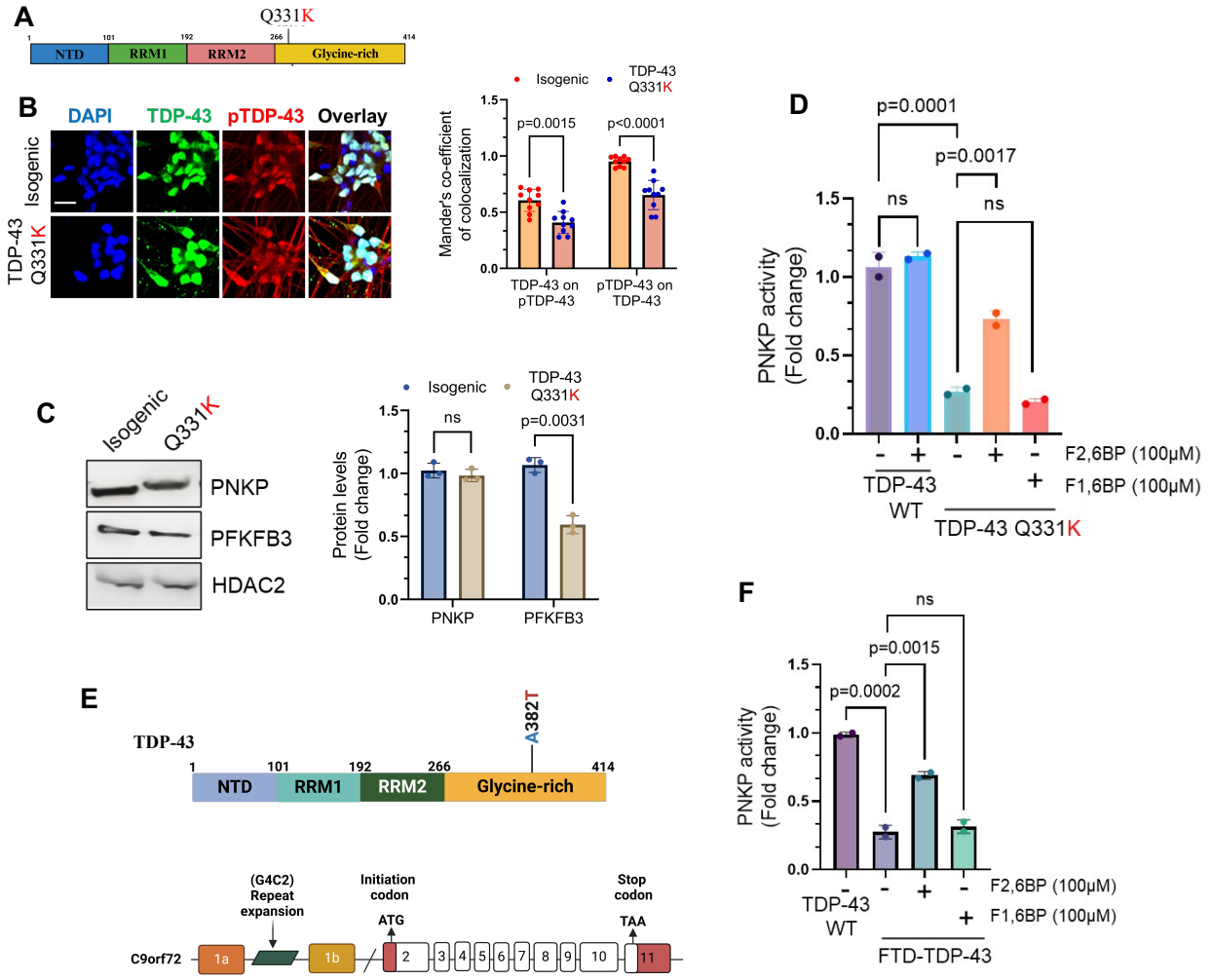

Supplementary Figure S2 (Related Figure 6). DNA Damage Induced by Mutant TDP-43 via PNKP Inhibition is Rescued by F2,6BP in ALS and FTD Patient Cell Lines.

A) Schematic representation of TDP-43 protein domains highlighting the Q331K mutation. The engineered iPSC line with Q331K mutation was obtained from Jackson laboratory.

B). IF analysis of Q331K mutant and isogenic control NPCs, showing cytosolic mislocalization of TDP-43 and its phosphorylated p409/410 form in the mutant cells. Mander's coefficient analysis quantifies colocalization between TDP-43 and pTDP-43, presented in the histogram.

C) IB analysis of WT and Q331K mutant cell nuclear extracts showing reduced PFKFB3 levels, while PNKP levels unaffected. HDAC2 served as nuclear loading control. Quantification of band intensities is shown in the histogram (*right panel*).

D) Quantitation of PNKP activity in nuclear extracts from Q331K mutant and WT NPCs, with or without F2,6BP. F1,6BP served as control.

E) Schematic representation of an FTD patient cell line harboring both TDP-43 (A382T) and an C9ORF72 repeat mutations.

F) Quantitation of PNKP activity in nuclear extracts from the FTD patient cell nuclear extracts, with or without F2,6BP. F1,6BP served as control.